Int. J. Electrochem. Sci., 11 (**2016**) 7401 – 7411, doi: 10.20964/2016.09.43

International Journal of
ELECTROCHEMICAL
SCIENCE
www.electrochemsci.org

Pt Heating Electrode for Microheater Based on Electrochemically Prepared Anodic Porous Alumina

Seungho Park[1,2], *Dongeun Lee*[1], *Sunghyun Byun*[1], *Hyeonseok Yoo*[3], *Dong-Wha Park*[3], *Woonsuk Hwang*[2,*], *Jinsub Choi*[3,*]

[1] Point Engineering, 89 Asan Valley-ro, Dunpo-myeon, Asan-si, Chungnam, South Korea
[2] Department of Metallurgical Engineering, Inha University, Yonghyun Dong 253, 402-751, South Korea
[3] Department of Chemistry and Chemical Engineering, Center for Molecular Catalysts and Applications (BK21 plus program), Inha University, Yonghyun Dong 253, 402-751, South Korea
[*]E-mail: wnshwang@inha.ac.kr, jinsub@inha.ac.kr

Received: 15 June 2016 / *Accepted:* 9 July 2016 / *Published:* 7 August 2016

Electrochemically prepared anodic aluminum oxide (AAO) was used as a supporting chip material for a microheater sensor, on which a patterned Pt electrode was deposited to generate resistive heat during current flow. Photolithography and a Pt/Ta sputtering process were conducted to prepare an interdigited electrode on the AAO supporting material. For efficient heat management within the heating zone, an air-gap ring was created around the heating zone using a chemical etching process. A thermal infrared camera image revealed that the generated heat is isolated within the heating zone. To achieve stable heating performance of the Pt layer, the Pt deposited on AAO was thermally annealed under various conditions. With increasing annealing temperature, the grain size of the Pt planes increased, leading to a highly stable Pt electrode on AAO. However, increasing the annealing temperature to 650°C resulted in the generation of pinholes, which led to degraded heating properties. A very small amount of heating power (50 mW) was consumed to maintain a heating zone temperature of over 600°C in the proposed AAO-based microheater.

Keywords: anodization, nanopores, microheater, Pt sputtering, supporting chip materials

1. INTRODUCTION

Recently, studies on state-of-the-art universal gas sensors [1-6], which can simultaneously detect various hazardous gases, have been actively performed because a trace amount of hazardous gas in a mixed gas can cause different environmental problems or significant catastrophic accidents in not only industrial regions but also residential areas [7-10]. Flammable gases and hydrocarbons can typically be detected by metal oxides, which usually operate under high temperatures in the range of

100–500°C [11]. Therefore, the installation of a good heater, which can accurately increase the temperature of the active sensing components up to the working temperature, is a crucial step in the preparation of highly sensitive gas sensors that consume a low amount of electricity [12-15].

Pt, which exhibits both high electric conductivity and thermal stability, is widely used as the heating electrode for microheater systems in gas sensor devices [16-18]. SiO_2 and Si_3N_4, which are often used as the supporting chip material for Pt, have poor adhesive properties; hence, several research groups have carried out investigations on the adhesive layer and the ideal annealing conditions for this layer [15, 18-20]. Yi's group claimed that Ta resulted in improved adhesive properties on Pt [21]. Tiggelaar et al. suggested that the use of a Ti adhesive resulted in diminished electrical features because of the atomic diffusion between Ti and Pt with annealing at 500°C [18]. Even though the Ta adhesive between the Pt electrode and the metal oxide microheater resulted in advanced adhesion properties with improved electrical conductivity, detailed information concerning the heat-treatment conditions remains unavailable [23, 24]

Anodic aluminum oxide (AAO), which exhibits a vertically high aspect ratio structure and highly ordered nanoporous arrays, has already been employed as one of the most popular host materials for molecular separation and sensing applications [25-27]. In gas sensing applications, AAO is widely employed to detect humidity changes based on the double layer created at the outmost oxide layer [27]. Furthermore, certain hazardous gases (e.g., NO_2, HCOH, and H_2O_2) can be accurately detected by the sensing materials built on an AAO supporter [28]. Recently, the use of AAO as a good alternative supporting chip material in place of Si_3N_4 or SiO_2 was successfully demonstrated, with AAO exhibiting comparative supporting chip properties at a low cost. For example, the heating power consumption for AAO to maintain a temperature of 450°C was approximately 2 times less than that for a silicon-based chip [29].

In this study, electrochemically prepared AAO substrates were used as the supporting chip material to enhance the thermal properties in the microheater for a sensor, in which Pt and Ta were employed as the heating electrode and adhesive material, respectively. A microelectromechanical system was used for the mass production of the microheater, which could be operated in the temperature range of 450–650°C. The microheating properties of Pt could be enhanced by careful design of the AAO-based microheater.

2. EXPERIMENTAL SECTION

2.1. Preparation of AAO substrates

A two-step anodization method was used to prepare the highly ordered AAO supporting chip material. The first anodic film was electrochemically prepared at 40 V over 1 h in 0.3 M oxalic acid and then removed by submersion for 2 h in a solution consisting of 1.8 wt.% CrO_3 and 6 wt.% H_3PO_4 at 50°C. Next, an AAO thin film with a thickness of 120 μm was prepared by a second anodization for 24 h in the electrolyte used in the first step. After the anodization, the Al substrate was removed from the AAO film in a mixture of 17 g $CuCl_2$ and 150 ml HCl (35%) in 850 ml of deionized (DI) water.

2.2. Fabrication of microheater

2.2.1. Patterning process for electrode

Photoresist (PR, ADEX-A05, DJ DevCorp) was spin-coated onto the AAO substrate at a rate of 0.3 m/min at 70–90°C and dried for 5 min in ambient air to allow formation of the pattern of the heater electrode by subsequent photolithography. The 12.5-mJ light under I-line conditions was exposed on the PR-covered AAO substrate for 8–11 s via the hard-contact method. After 1 h of the holding procedure, the substrate was treated using a post-exposure bake (PEB) process at 80°C for 3 min. The exposed PR layer was removed in cyclohexanone as the developer by the mixed process of dipping and spraying for 60–90 s. All the wafers were rinsed and dried with isopropyl alcohol (IPA) using a spin coater.

2.2.2. Deposition process for electrode

The patterned AAO was baked at 50°C in an oven to remove the water that might be present in the nanoporous channels. The Pt (6.75-inch diameter, 3-mm thickness, 99.95% purity) and Ta (6.75-inch diameter, 7 mm thickness, 99.95% purity) targets, which were installed in the sputter chamber, were sputter-deposited onto the patterned structure on AAO. The base pressure was maintained under 3.0×10^{-7} Torr. For the Ar plasma, 20 sccm of Ar was injected in the chamber, and subsequently Ta and Pt were deposited onto the patterned structure on AAO using an ion gun under the 2.0×10^{-3} Torr of process pressure at a substrate temperature of 23°C. For uniform ion cleaning, the turntable attached to the AAO wafer was rotated at 0.5 rpm at 1000 V in collimated mode.

Pre-sputtering was performed to exfoliate the native oxide thin film for all the metal targets to sustain a stable plasma state in the chamber at 200 W for 1 min. The deposition power values for Ta and Pt were 15 W (deposition rate of 4.75 Å/s) and 40 W (deposition rate of 2.27 Å/s), respectively. The heater was annealed at temperatures of 450°C, 550°C, and 650°C to confirm the effect of the heat treatment on the microheater electrode.

2.3. Air-gap formation

For fabrication of the air-gap pattern, the photolithography process was used again. After developing a process to remove the patterned air-gap, the exposed aluminum oxide was selectively removed in a solution consisting of 1.8 wt.% CrO_3 and 6 wt.% H_3PO_4 at 50°C for 60 min. The cleaning step of the air-gap-formed AAO was performed with IPA and DI water for 10 min, successively.

2.4. Morphological analysis

The morphology of samples was characterized with focus ion beam assisted field emission scanning electron microscope (FIB-SEM, NOVA200, FEI, Netherlands). For the clear cross-sectional image through FIB section, Pt/C layer was coated on the top of Pt/Ta layer on AAO under the same

conditions for the preparation of Pt/Ta layer. X-ray diffraction (XRD, Ultima iii, Rigaku, Japan) was used to determine the grain size distribution of Pt/Ta layer through full width at half maximum (FWHM) analysis; FWHM was calculated through the software (MDI Jade 6.2.9200) supplied by the XRD company.

2.5. Performance test for microheater

A thermal imaging camera (A655sc, FLIR, USA) was installed to measure the thermal performance of the microheater. The heater was aligned in front of the lens of the camera on the alignment stage. To obtain more accurate information, the magnifying function of the camera was applied for precise alignment between the camera lens and heater. After the alignment, the sample was monitored in real time while voltage was applied using DC power supply (SourceMeter 2420, Keithley). The temperature of the sample was measured to determine the thermal stability when the voltage was changed. Based on the thermal imaging camera, temperature vs. power, temperature vs. operating time, and current transient as a function of time were precisely determined.

3. RESULTS AND DISCUSSION

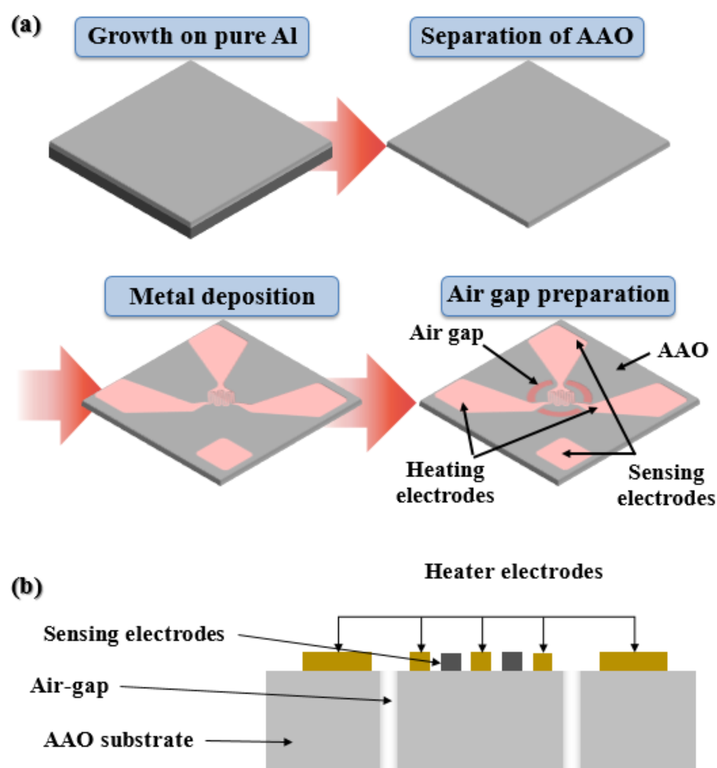

Figure 1. Schematic diagram of the fabrication procedures for Pt electrode on AAO supporting chip: (a) AAO growth on Al → separation of AAO from Al → Pt electrode formation on AAO through photolithography process and Pt sputtering → air-gap formation through photolithography and

chemical selective etching of AAO and (b) cross-sectional image.

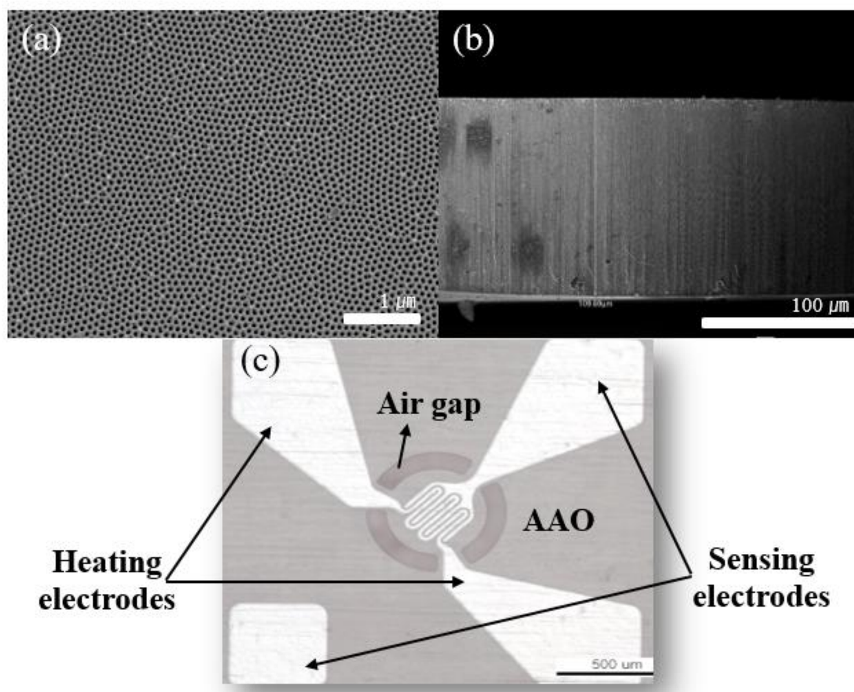

Figure 2. Photographs of Pt electrode on AAO for sensing microheater. (a) Top view and (b) cross-sectional view of anodic porous aluminum oxide supporting chip. (c) Pt electrode and air-gap patterned AAO microheater.

Figure 1 presents a schematic diagram of the fabrication of the microheater based on AAO. First, an anodic oxide was grown on an Al substrate, and subsequently, the AAO was separated from the Al substrate. Then, through photolithography and sputtering of Pt, a Pt deposit was formed on the AAO. Herein, the Pt and AAO played the roles of the heating electrode, in which resistive heat was generated during current flow, and the supporting material, in which thermal energy was effectively isolated by the porous structure, respectively. An air-gap ring was created around the heating zone to further improve the efficiency of the thermal properties of the microheater. Notice that most works on the fabrication of microheater based on AAO was designed without the air-gap due to technical difficulty [28-29]. Photolithography and chemical etching process was successfully done for the air-gap for the isolation of heat within the heating zone. A sensing electrode interdigited with the heating electrode was prepared to measure the current change when the sensing element detected the target gas. A photograph of the microheater is presented in Figure 2.

The supporting material is nanoporous anodic alumina with a pore diameter of 35 nm and a thickness of 120 μm, which is the typical anodic structure prepared in oxalic acid [30]. The width of the heating electrode was narrowed in the heating zone, leading to the generation of resistive heating during current flow. The sensing electrode interdigited with the heating electrode and air-gap ring around the heating zone are clearly observed in the photograph. The total heating zone area is less than 500 μm in diameter. Figure 3 shows that the heat distribution is typically concentrated in the heating zone in real operation at 3 V because of the air gap. The heating zone exhibits a uniform temperature distribution of approximately 725°C, whereas a value of less than 200°C was measured outside of the

heating zone. This result indicates that heat is well managed within the heating zone, suggesting efficient heating power consumption (50 mW). It has been reported that at least 200 mW is required for keeping the heating zone temperature by the conventional Al_2O_3 based supporting material [29].

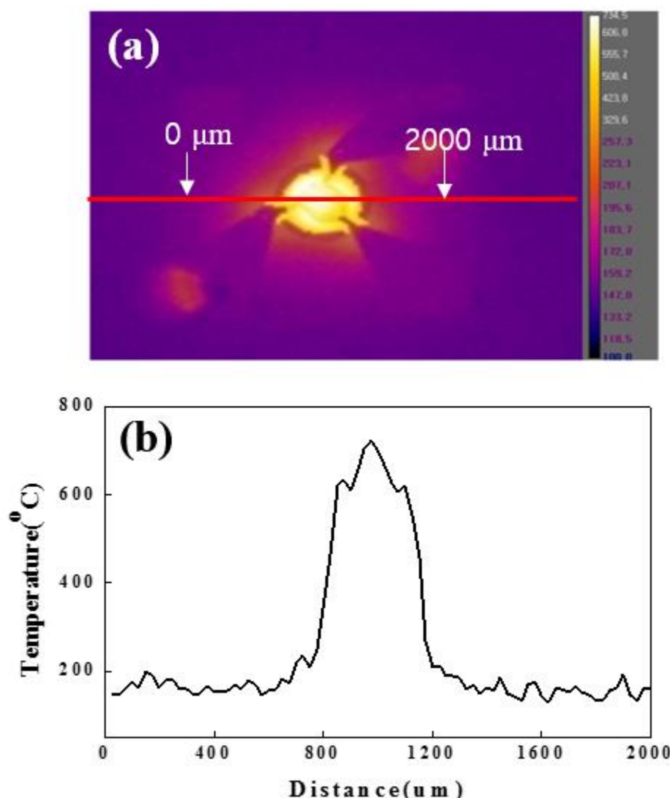

Figure 3. (a) Thermal infrared camera image showing heat distribution on the Pt electrode generated at 3 V (50 mW). (b) Graphical images of heating distribution along line A in (a).

Table 1. FWHM analysis of grain size of different Pt planes as a function of annealing temperature.

2-theta	Miller-index	FWHM				Grain size(Å)			
		AS	450℃	550℃	650℃	AS	450℃	550℃	650℃
39.826	(111)	0.346	0.280	0.250	0.256	268	351	411	399
46.326	(200)	0.622	0.392	0.348	0.329	142	234	269	287
81.483	(311)	1.049	0.643	0.499	0.521	100	166	216	206
85.963	(222)	0.791	0.513	0.429	0.408	138	217	263	278

To fabricate a reliable heating electrode, the Pt layer on AAO was thermally annealed under various annealing conditions. Figure 4 presents X-ray diffraction (XRD) data of the annealed Pt on AAO, revealing the appearance of four peaks at 39.8°, 46.4°, 81.48°, and 85.9°, which are indexed to the (111), (200), (311), and (222) planes, respectively [31]. All the samples exhibited a (111) peak with

strong intensity, whereas the intensities of the other peaks were very weak. From full-width-at-half-maximum (FWHM) analysis of the peaks, we deduced the grain size of the four different planes of Pt. All the results indicate that the grain size of Pt increased up to 550°C and the size of some of the planes decreased upon further increasing the annealing temperature (see Table 1). A scanning electron microscope (SEM) equipped with a focused ion beam (FIB) was used to finely prepare a cross-sectional image.

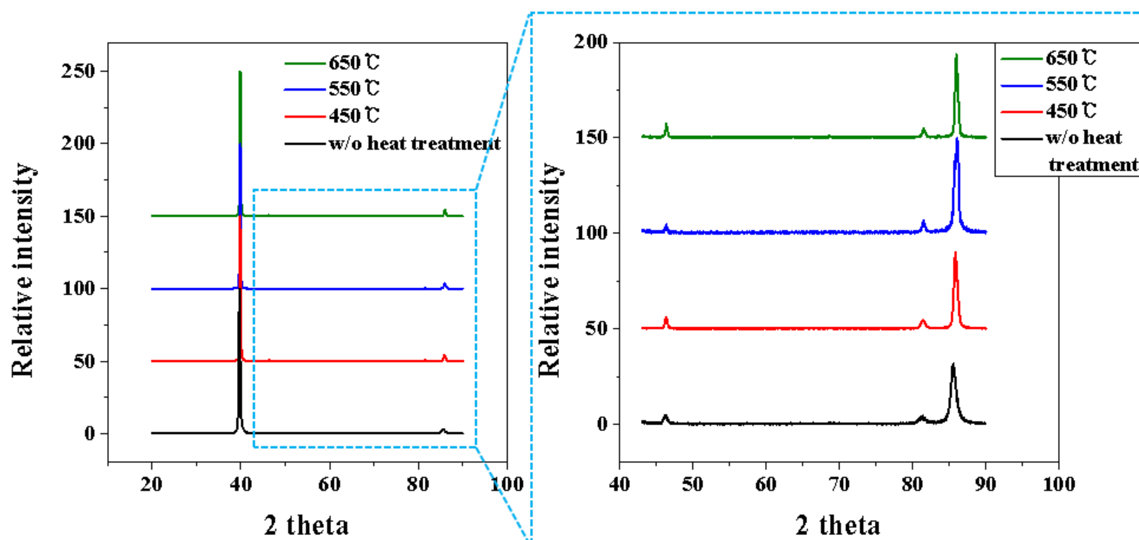

Figure 4. XRD analysis of the Pt electrode patterned on AAO. The samples were annealed at 450°C, 550°C, and 650°C. An enlarged view of the range from 40° to 90° is shown on the left side.

Figure 5 presents cross-sectional images of the Pt coated layer after FIB operation, demonstrating that the thickness of the Pt coating layer increased from approximately 740 nm in the as-prepared Pt on AAO to 845 nm after the 650°C annealing. Note that the outermost layer is a Pt/C layer for FIB sectioning. These findings can be explained by the fact that the grain size gradually increased with increasing annealing temperature. Notably, distinguishable pinholes of Pt layers were observed when the annealing temperature reached to 650°C, indirectly indicating that the different thermal expansions of Pt/Ta/AAO lead to a stress between the layers. In addition, it has been reported that Pt atoms are easily diffused into other neighbor layers over 600°C. The rich and excess Pt atoms can easily make the flow through grain boundary to other layers owing to the high atomic mobility of Pt at a high temperature. [18, 32-34]. Thus, it is clearly expected that a high annealing temperature (herein, 650°C) might lead to inferior performance of the heating electrode. Figure 6 shows the typical temperature changes in terms of applied power in the heating electrode, which is controlled by applying a constant voltage and corresponding current. To obtain a power of 50 mW, the applied voltage was increased from 1 mV to 3 V. Because the requirement of low power to reach the target temperature is a significant benefit for mobile applications, the maximum applied voltage we used was less than 3 V. Figure 6 clearly demonstrates that the temperature of the heating electrode can be accurately controlled by modifying the external applied power in the range of a few mW.

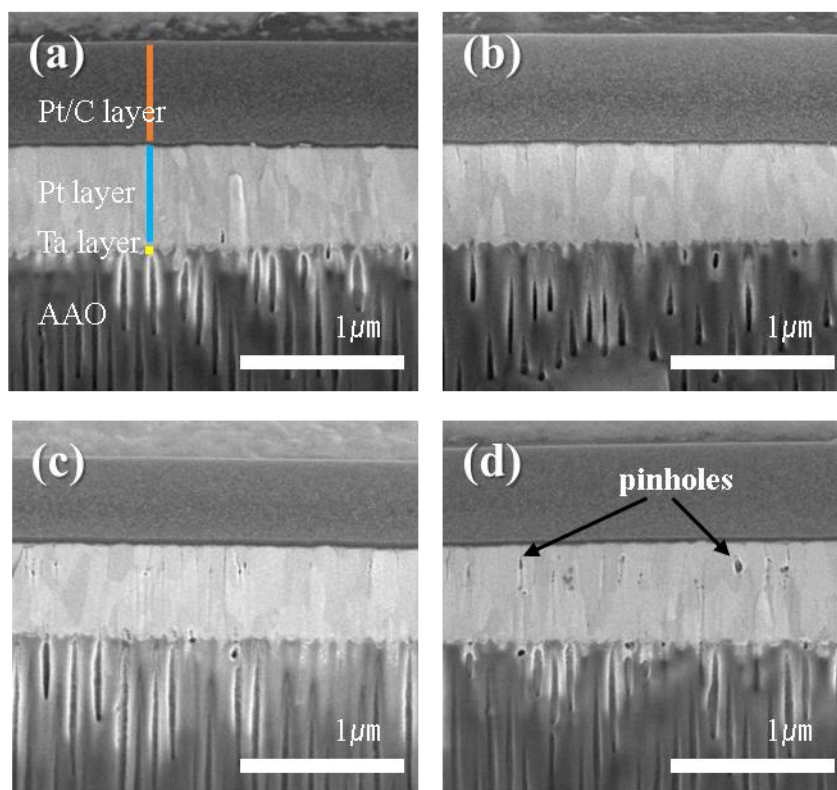

Figure 5. High-resolution cross-sectional scanning electron microscopy (SEM) images of Pt electrode on AAO: a) as-prepared and after annealing at (b) 450°C, (c) 550°C, and (d) 650°C. Notice that there are 3 typical layers shown; Pt/C, Pt/Ta and AAO. Distinct pinholes are observed in Fig.5 (d)

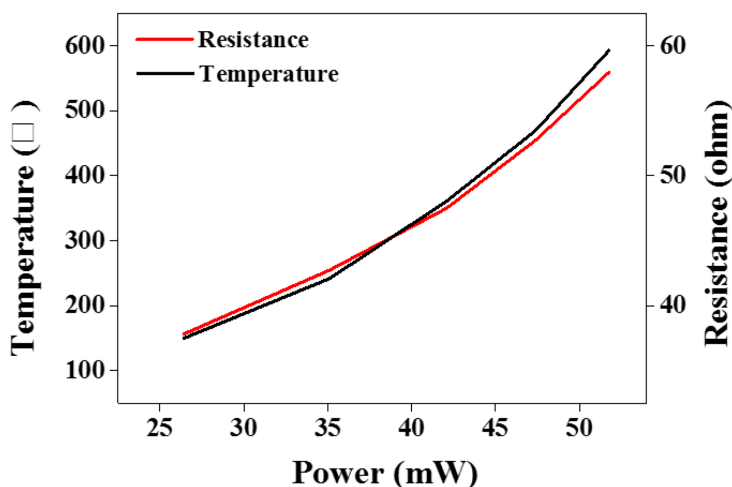

Figure 6. Temperature generated by resistive heat during current flow. The temperature is controlled by the heating power.

Figure 7 presents temperature profiles as a function of operation time at constant applied voltage (3 V), demonstrating that the unannealed and low-temperature-annealed (450°C) samples exhibited strong fluctuations of temperature (unstable mode) during the operation time, whereas a relatively small temperature change was observed for the samples annealed at 550°C and 650°C. The

highest average temperature of 725°C at the applied voltage of 3 V was achieved in the 550°C-annealed samples, indicating that the most stable/compact Pt layer and interface between Pt and AAO was obtained for this annealing condition. Because a constant voltage was applied to the heating electrode, resistance formed, which led to a reduction of the current flow during heating.

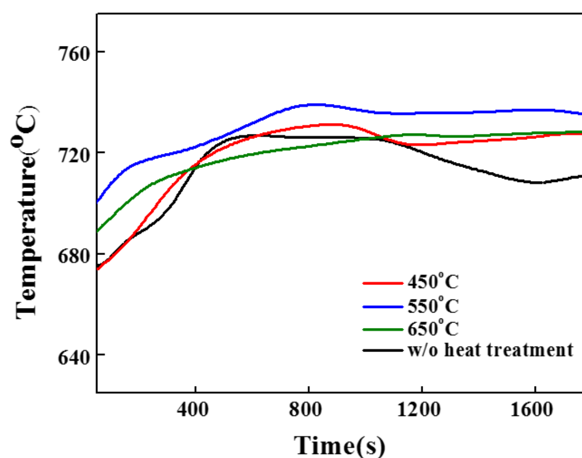

Figure 7. Temperature transient as a function of operating time. A constant voltage of 3 V was applied during the operation.

Figure 8 demonstrates that the current difference deviated from the initial current as a function of the operation time. For the unannealed sample, the current was significantly reduced during the heating, indicating the formation of substantial resistance due to the oxidation of Pt and thermal stress between Pt and AAO. The resistance was greatly reduced if the Pt layer was annealed under appropriate conditions. A very small deviation of current was observed for the 550 °C sample, indicating again that an annealing temperature of 550°C is optimal.

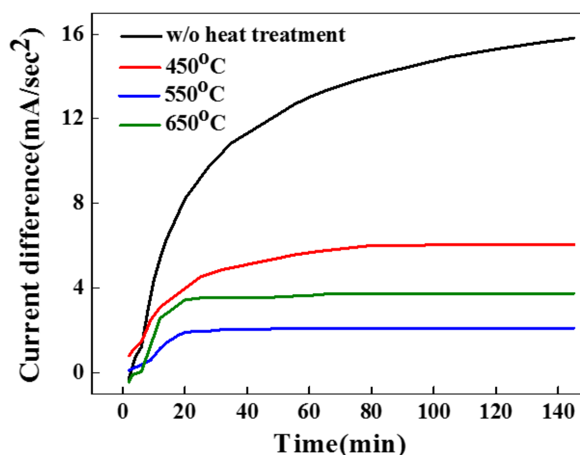

Figure 8. Deviation of current difference from the initial operation at a constant applied voltage of 3 V.

4. CONCLUSIONS

We demonstrated that electrochemically prepared highly ordered AAO can be successfully used as a supporting chip material for Pt electrodes, which generate resistive heat during current flow. To achieve good adhesion between the Pt electrode/Ta buffer layer/AAO, the prepared samples were annealed under various conditions; the annealing temperature of 550°C resulted in the optimal resistive heat generation. The average heat generated at 3 V was measured to 725°C, and a very stable temperature change was observed during operation under this condition. This finding was due to the grain size change as a function of annealing temperature; the maximum grain size of Pt was observed for the 550°C annealing temperature. A further increase in the annealing temperature led to the formation of pinholes in the layer because of the different thermal expansions as well as Pt diffusion problem. In addition, the air-gap design provided effective heat isolation in the heating zone, consuming a very small amount of heating power (50 mW) to maintain the sensing temperature of 725°C.

ACKNOWLEDGEMENTS
This research was supported by the Ministry of Trade, Industry & Energy(MOTIE), Korea Institute for Advancement of Technology(KIAT) through the Encouragement Program for The Industries of Economic Cooperation Region.(R0004909, Develop of AAO Material for the Diffuser Function for Display and Semiconductor CVD)

References

1. W. Moritz, U. Roth, M. Heyde, K. Rademann, M. Reichling, J. Hartmann, *Thin Solid Films* 391 (2001) 143.
2. S.Z. Ali, F. Udream W.I. Milne, J.W. Gardner, *J. Microelectromech. Syst.* 17 (2008) 1408.
3. C.Y. Lin, Y.Y. Fang, C.W. Lin, J.J. Tunney, K.C. Ho, *Sens. Actuators B* 146 (2010) 28.
4. T. Waltz, B. Becker, T. Wagner, T. Sauerwald, C.D. Kohl, M. Tiemann, *Sens. Actuators B* 150 (2010) 788.
5. H.G. Moon, H.W. Jang, J.S. Kim, H.H. Park, S.J. Yoon, *Sens. Actuators B* 153 (2011) 37.
6. M.R. Mohammadi, D.J. Fray, *Acta Mater.* 55 (2007) 4455.
7. N. Yamazoe, *Sens. Actuators B* 180 (2005) 2.
8. D.R. Miller, S.A. Akbar, P.A. Morris, *Sens. Actuators* B 204 (2014) 250.
9. Y. Shimizu, M. Egashira, *MRS Bull.* 24 (1999) 18.
10. C.W. Na, H.S. Woo, I.D. Kim, J.H. Lee, *Chem. Commun.* 47 (2011) 5148.
11. E.Yoon, *Sens. Actuators B* 2 (1990) 63.
12. S.V. Patel, M. DiBattista, J.L. Gland, J.W. Schwank, *Sens. Actuators B* 37 (1996) 27.
13. D. Briand, F. Beaudoin, J. Courbat, N.F. de Rooij, R. Desplats, P.Perdu, *Microelectron. Reliab.* 45 (2005) 1786.
14. J. Courbat. D. Briand, N.F. de Rooij, *Sens. Actuators A* 142 (2008) 284.
15. H. Esch, G. Huyberechts, R. Mertens, G. Maes, J. Manca, W. De Ceuninck, L. De Schepper, *Sens. Actuators B* 65 (2000) 190.
16. D. Resnik, D. Vrtacnik, M. Mozek, B. Pecar, S. Amon, *J. Micromech. Microeng.* 21 (2011) 025025.
17. P. Swaminathan, D.A. LaVan, T.P. Weihs, *J. Appl. Phys.* 110 (2011) 113519.
18. R.M. Tiggelaar, R.G.P. Sanders, A.W. Groenland, J.G.E. Gardeniers, *Sens. Actuators A* 152 (2009) 39.
19. T.C. Tisone, J. Drobek, *J. Vac. Sci. Technol.* 9 (1971) 271.

20. A. Ehrlich, U. Weißner, *Thin Solid Films* 300 (1997) 122.
21. F. Yi, W. Osborn, J. Betz, D.A. LaVan, *J. Microelectromech. Syst.* 24 (2015) 1185.
22. T. Maeder, L. Sagalowicz, P. Muralt, *Jpn. J. Appl. Phys.* 37 (1998) 2007.
23. M. Chen, L.D. Schmidt, *J. Catal.* 55 (1978) 348.
24. Y.F. Chu, E. Ruckenstein, *J. Catal.* 55 (1978) 281.
25. L. Yao, M. Zheng, H. Li, L. Ma, W. Shen, *Nanotechnology* 22 (2011) 379501.
26. C.K. Chung, O.K. Khor, C.J. Syu, S.W. Chen, *Sens. Actuators B* 210 (2015) 69.
27. Y. Kim, B. Jung, H. Lee, H. Kim, K. Lee, H. Park, *Sens. Actuators B* 141(2009) 441.
28. A. Santos, T. Kumeria, D. Losic, *Trends Anal. Chem.* 44 (2013) 25
29. A.A. Vasiliev, A.V. Pisliakov, A.V. Sokolov, N.N. Samotaev, S.A. Soloviev, K.Oblov, V. Guarnieri, L. Lorenzelli, J. Brunelli, A. Maglione, A.S. Lipilin, A. Mozalev, A.V. Legin, *Sens. Actuators B* 224 (2016) 700.
30. H. Masuda, H. Yamada, M. Satoh, H. Asoh, *Appl. Phys. Lett*. 71 (1997) 2770
31. K. Shimizu, I. F. Cheng, J. S. Wang, C. H. Yen, B. Yoon, C. M. Wai, *Energy Fuels* 22 (2008) 2543.
32. L. Xiao, Z. Zhao, L. Du, S. Wu, Q. Liu, Annealing effect on stability of platinum thin films covered by SiO_2 Or SiN_x Layer, *NEMS2013*, Suzhou, China, 2013, 352.
33. M. Grosser, U. Schmid, *Appl. Surf. Sci.* 256 (2010) 4564
34. E. Chason, B. W. Sheldon, L. B. Freund, *Phys. Rev. Lett.*, 88 (2002) 156103.

© 2016 The Authors. Published by ESG (www.electrochemsci.org). This article is an open access article distributed under the terms and conditions of the Creative Commons Attribution license (http://creativecommons.org/licenses/by/4.0/).